Proceedings of IMECE2005:
2005 ASME International Mechanical Engineering Congress and Exposition
November 5-11, 2005, Orlando, Florida USA

IMECE2005-81153

MODELING AND CHARACTERIZATION OF DIELECTROPHORETIC ASSEMBLY PROCESS FOR NANOBELTS

Peter J. Hesketh
Georgia Institute of Technology
Mechanical Engineering
801 Ferst Dr., Atlanta, GA 30332-0405 USA
404-385-1358, peter.hesketh@me.gatech.edu

Martha A. Gallivan
Georgia Institute of Technology
Chemical and Biomolecular Engineering
311 Ferst Dr., Atlanta, GA 30332-0100 USA
404-385-1358, martha.gallivan@chbe.gatech.edu

Surajit Kumar
Georgia Institute of Technology
Mechanical Engineering
801 Ferst Dr., Atlanta, GA 30332-0405 USA

Christine J. Erdy
Georgia Institute of Technology
Chemical and Biomolecular Engineering
311 Ferst Dr., Atlanta, GA 30332-0100 USA

Zhong L. Zhang
Georgia Institute of Technology
Materials Science and Engineering
771 Ferst Dr., Atlanta, GA 30332-0245 USA
404-894-8088, zhong.wang@mse.gatech.edu

ABSTRACT

Robust manufacturing methods are needed for nanocomponent assembly, and one must understand the physics to optimize the processing and to develop control schemes to deal with the inherent uncertainty. We are studying field induced assembly of a new class of semiconducting metal oxides – nanobelts – that have been demonstrated for chemical sensing. We have demonstrated the integration of nanobelts with electrodes to make sensors by dielectrophoresis (DEP). The SnO_2 nanobelts (width ~ 100 - 300 nm, thickness ~ 30 - 40 nm) were suspended in ethanol and introduced into a microchannel, and were assembled across the electrodes. Modeling suggests that attraction should occur at all frequencies over this range. Targeted experiments were performed to quantify surface and material properties for input to the modeling, and FEMLAB simulations were performed to validate the model. The goal of the modeling is to optimize the assembly of nanostructures in a manufacturing process at the wafer-scale.

INTRODUCTION

A fascinating range of new materials with previously unattainable properties are being developed by nanoscientists. Applications of these new materials include nanowire-based electronics, nanosensors, optical systems, flat panel displays that use carbon nanotubes, high heat flux modified surfaces and biological and biomedical applications. However, the assembly of these nanostructured materials into nanometer-scale devices that impact our everyday lives has not yet followed, in part due to the difficulty in assembly of such materials in a repeatable manner necessary for manufacturing.

We suggest that scientists and engineers must work together to develop manufacturing processes for nanoscale devices. Various application areas and disciplines have developed their own frameworks for manufacturing, including mechanical engineering, chemical engineering, and the integrated circuit industry. Each begins with the relevant manufacturing steps, models them separately, and then determines how to incorporate them to optimize yield and reduce cost. We wish to address a portion of the nanomanufacturing framework, specifically those issues associated with the assembly of nanostructures. In particular, we are developing and validating physical models for field-induced assembly, and which will then be used to improve or even optimize device performance and manufacturing yield.

The assembly of nanostructures is critical if they are to be used in devices. One option is to grow the structures in the actual device. For example, carbon nanotubes can be directed through catalytic processing to assemble on silicon oxide surfaces [1]. The advantage of assembly after growth is that the processing conditions for the nanostructure formation are not limited by the bulk substrate material and its extent. However, subsequent assembly and size selection may be necessary prior to deposition onto the substrate or device. Assembly may be directed by biological binding with

oligonucleotides [2], or by local fluid dispensing in the case of nanofluidic droplet dispensing [3], or by dielectrophoreis for which we have obtained preliminary results. Each of these methods has processing characteristics and inherent limitations. A quantitative approach is needed to develop robust manufacturing methods for nanocomponent assembly, and to understand, characterize, and develop control schemes to deal with the inherent uncertainty in the processing.

The characteristics of the fluid-based assembly processes might well be analyzed within the manufacturing framework developed for integrated circuits. In particular, the mode of manufacture of nanodevices might expand on the concept of fault tolerance that has been applied extensively to integrated circuit manufacture for yield evaluation and prediction [4,5]. Models of the manufacturing processes, including probabilistic models of disturbances, may bear some similarity to those used to describe defect analysis as it applies to the design of fault tolerant integrated circuits. Can these methods for designing in the presence of inherent uncertainty also be applied to the manufacture of nanoscale devices? Despite the fluctuations associated with the self-assembly of nanowires, nanobelts, or other nanostructures, it may be possible to design redundant devices that can be manufactured with high yield. It may also be possible to add reconfiguration steps in which additional processing is performed on unacceptable devices.

DIELECTROPHORESIS

Dielectrophoresis (DEP) is defined as the polarization and associated motion induced due to the effect of an inhomogeneous electric field. The induced motion is determined by the dielectric properties of the nanowire or particle, unlike electrophoresis where motion of the particle or nanowire is determined by the magnitude and polarity of the net electrical charge. Both alternating current (AC) and/or direct current (DC) electric fields may be employed. Also the DEP effect is independent of the charge on a nanowire, so that a neutral nanowire can be subject to this effect, making it more versatile in its application to nanowire separation and assembly. There are two different effects associated with DEP: positive and negative DEP. Positive DEP occurs when the nanowire is more polarizable than the medium, causing the wire to be attracted to maxima of the electric field intensity. The reverse is true for negative DEP. Manipulation of particles and in particular biological cells, viruses and proteins has been reported utilizing dielectrophoresis and a comprehensive review is given by Burke [6]. Dielectrophoresis was pioneered with the early work of Pohl in the 1950's. His book and the text by Pethig [7] on biological application provide the foundation for this field. More recent text by Jones [8] focuses on particles, and the application of dielectrophoresis to manipulation and sorting of bioparticles is reviewed by Huang *et al.* [9].

The DEP forces on an object are generated by gradients in the electric field. Interdigitated electrode arrays (IDA) are a frequently selected method for producing high electric field gradients, and as the electrode spacing is reduced the field is proportional to the inverse of the gap. Modeling of the field distribution in this simple geometry has been solved analytically with the Schwartz-Christoffel transformation [10]. Others have used finite element analysis to determine field distribution, because the effect of polarizable material in the fluid can also be included and because more complex electrode geometry can be considered [11].

The DEP forces on an object can be calculated by directly integrating the charge and electrical field over the object, or can be approximated with simpler equations using the dielectrophoretic approximation and the effective moment method [7]. It is important to note that these approximations are derived by assuming that the electric field changes only slightly across the objects. While this approximation is reasonable for a small particle, it clearly is not justified in our application, since the nanobelt length is similar to the electrode spacing (20 μm). The dipole approximation for a spherical particle is

$$\mathbf{F}_{DEP} = 4\pi R^3 \,\mathrm{Re}(\varepsilon_f)\,\mathrm{Re}(K)\nabla(\mathbf{E}^2) \tag{1}$$

where R is the radius of the particle, ε_f is the electrical permittivity of the fluid, and $\mathbf{E}$ is the local electric field. The Clausius-Mossoti factor K for a spherical particle is

$$K = \frac{\varepsilon_p - \varepsilon_f}{\varepsilon_p + 2\varepsilon_f} \tag{2}$$

where ε_p is the complex electrical permittivity of the particle. Analogous expressions have also been derived for ellipsoidal particles, but still require the dipole assumption (the particle dimensions are small relative to the changes in the electric field). Note that the externally applied electric field must already be known in order to use equations (1). This field is known for the IDA electrodes discussed in the previous paragraph, or can be computed numerically using equation (6).

PRIOR WORK ON NANOWIRE ASSEMBLY

Several groups have demonstrated the manipulation and assembly of metallic nanowires and carbon nanotubes at microelectrodes utilizing DEP [12,13,14]. The selective transport of the nanowires to the electrode surface is a function of their dielectric properties. One of the earliest reports is on the purification and alignment of carbon nanotubes with AC field in isopropyl alcohol by Yamamoto *et al.* [15]. Longer nanotubes were observed to have the greater degree of orientation at a high frequency of 10 MHz (compared to 10 Hz). The rapid assembly of metallic nanowires was demonstrated by Smith *et al.* [16] and directed placement of carbon nanotubes has also been shown in an aqueous medium [17]. The electrode material has been observed to influence carbon nanotube manipulation [18]. Alignment with DC fields was demonstrated by Kumar *et al.,* [19] where attraction to the anode suggests a negative charge on the carbon nanotube. However, alignment is, in general, improved with a mixed AC and DC field [20]. Chung and Lee [21] demonstrated assembly of a single carbon nanotube at 20 nm gap electrodes. The electrode tip radius had a strong influence on the assembly and alignment of the nanotubes [22]. Separation and enrichment of metallic from semiconducting carbon nanotubes has been demonstrated by Chen *et al.* [23] and Lee *et al.* [24] in a liquid droplet on chip. After 7 cycles an enrichment of 95% was achieved. Assembly at individual nanometer scale electrodes has been demonstrated by Jin *et al.* [25] for the organization of nanowires to build electronic devices at 300 nm spaced electrodes with a success rate of 90%.

PROJECT DESCRIPTION

Metal oxides are commonly used for detecting flammable and toxic gases, including organophosphosphorus compounds [26] (e.g. nerve agents), halogenated hydrocarbons, CO, NO_2, NH_3, CH_4, H_2, H_2S, alcohols, O_2, and ozone. The sensing mechanism is based on a surface oxidation-reduction (redox) process that changes the concentration of oxygen vacancies in the metal oxide and thus alters its electrical conductance [27,28]. Because only the surface layer is affected by the reaction, the sensitivity of a metal oxide sensor increases for decreasing thickness, motivating the development of thin film metal oxide sensors with the use of MEMS technologies [29].

Several groups have demonstrated nanowires [30], nanobelts [31], and carbon nanotubes [32] can function as chemical and/or biosensors [33, 34,35,36]. Tin oxide nanobelt device can be used for CO, ethanol and NO_2 sensing [31]. Very high sensitivity down to ppb levels has been observed in sensing NO_2 [33] using In_2O_3 nanowire devices. Several mechanisms of transduction are reported for these devices, including field effect, conductiometric or capacitive mechanisms. There is however a strong coupling with the surface adsorbate on the nanowire or nanotubes. Alternative methods of transduction include enthalpy, surface energy, field emission and electron tunneling, several of which have been successful in dispersed nanoparticle film sensors. Whether greater sensitivities can be achieved compared to the counterpart "microsensor" of similar transduction mechanism is still an unresolved question. However, if the depletion region in the nanowire sensor is comparable to the cross-sectional area then a greater conductance modulation has been demonstrated [37]. The important aspects of reversibility, hysterisis, reproducibility, selectivity, and base line drift also need to be addressed before the benefits of this nanotechnology can be fully realized. Finally, analyte matrix effects and poisoning of the sensor interface need careful characterization. In any case, nanosensors have the promise of low power, small size and redundancy in an array format.

Nanowire arrays could potentially be assembled one wire at a time, using an AFM probe, but that would not be scalable to a high-throughput manufacturing process. Instead, we consider field-induced assembly, using dielectrophoresis, flow, and gravity. Brownian motion may also add significant noise to the assembly process, depending on the process design and the nanowire dimensions. In order to build a selective gas sensor, wires with different properties are need. One could individually functionalize the wires after assembly using dip-pen lithography, but that would not scale well for high-throughput. In our project we plan to flow in different wires at different times into the chamber, to assemble them in different areas on the electrode array. We may also mask off areas at various times using PDMS molds.

EXPERIMENTAL PROCEDURE

SnO_2 nanobelt samples were made using the thermal evaporation method outlined in [38,39,40]. This process utilizes a condensed powder source material which is vaporized at elevated temperatures and the resultant vapor is condensed to form the desired product. The process was conducted in a tube furnace. The carrier gas enters the alumina tube and is pumped out by the rotary pump. The source material is loaded on an alumina boat and positioned at the center of the alumina tube. Several alumina plates (60 mm x 10 mm) were placed downstream, one behind the other, inside the alumina tube, which acted as a substrate for collecting growth products. After the alumina tube is evacuated to ~$2x10^{-3}$ torr, thermal evaporation of SnO powder (purity 99.9 %, melting point 1080 ^oC) was conducted at ~ 1050 ^oC for 2 hours, under a pressure of 200 - 600 torr and an Ar carrier gas flow of 50 sccm. The substrate temperature was carefully controlled for the products to deposit on it. The same nanostructure can also be made at 1350 ^oC from SnO_2 powder (purity 99.9 %, melting point 1630 ^oC).

Details of the electrode fabrication have been described previously [41]. To summarize, the Au electrodes with a Ti adhesion layer are built on 1000 μm thick Pyrex glass (*G.M. Associates Inc.*, Oakland, CA, USA) substrates (or wafers). The glass is transparent to allow visualization of the flow using an inverted microscope. The 300 Å thick titanium (Ti) layer, and 2500 Å thick gold (Au) layer were deposited using an e-beam evaporation. The pattern of the electrodes is castellated to enhance lateral DEP forces. The minimum gap between the electrodes was fixed at 20 μm. Two sets of electrode pairs are defined in each measurement cell. An SU-8 spacer is spin coated and UV exposed producing a spacer layer of 80 μm thickness after development. Electrical contacts are made with conductive silver epoxy (Loctite 3880, *Henkel Consumer Adhesives*, Avon, OH) and then coated with insulating epoxy (Loctite Extra Time) to provide additional strength and insulate the contacts. This electrode array is pictured in Figure 1.

Figure 1. Completed electrode array with SU-8 layer to define measurement volume.

The nanobelt product obtained from the furnace is an agglomerate, with the individual nanobelts intertwined with each other. The individual nanobelts are separated by sonication in ethanol. The lengths of the nanobelts vary depending on the sonication time; short nanobelts (lengths of a few μm's) and long nanobelts (lengths of 10's of μm's) are produced after sonication. The nanobelts used in the tests had a width in the range of 100 - 300 nm, so that it could be observed under an optical microscope as a dark line. One atomic force microscope (AFM) measurement showed it to be 30 - 40 nm thick. Separate SEM measurements on the nanobelt sample have also confirmed that the thickness is in that range, although not all the nanobelts are of the same thickness. The thickness is

also determined by the conditions under which the nanobelts were made from the evaporation process.

The sample is sonicated for a few minutes prior to injection with a syringe. Approximately 5 μL was injected into the cell with a SU-8 mold surrounding the measurement area and the glass cover placed over the cell. Figure 2 shows a cross-section of the measurement cell and the location of the microscope.

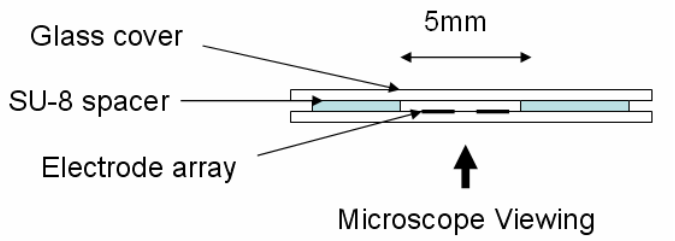

Figure 2. A schematic diagram indicating the experimental set up for observing the nanobelt motion over the electrodes.

Observation was carried out using an inverted microscope, Nikon Eclipse TE2000-S (*Nikon Instruments Inc.*, Melville, NY, USA). The nanobelts could be seen as dark lines under the microscope. An AC voltage of 20 V peak to peak (7.07 RMS) was applied between the electrodes using a Synthesized Function Generator (*Stanford Research Systems Inc.*, Sunnyvale, CA, USA). The frequency was varied from 0.1 Hz to 10 MHz and the effect on the nanobelts and nanoparticles was observed. Digital images were taken using a computer controlled imaging software, MetaMorph® Imaging System (*Universal Imaging Corporation*, Downingtown, PA, USA), which enabled automated image capture and analysis from a digital CCD camera attached to the microscope. Digital movies were also recorded showing the movement and alignment of nanobelts in response to different frequency ranges of the applied AC voltage.

MODELING

The goal of our modeling is to express the force and torque on a nanobelt as a function of wire position and orientation, and then to compute the nanobelt trajectories during the assembly process as a function of the applied potential and the initial wire position and orientation in the inlet stream. The interaction between nanobelts is neglected in the current model, since we plan to operate with a dilute concentration of wires. The approach now is to consider a distribution of wires in the inlet stream, and to compute their individual trajectories (either passing through the channel or depositing on the electrodes) to obtain the final distribution of the nanobelts.

The forces on a wire include contributions from various fields, including flow, gravity, and electric field:

$$F_{total} = F_{drag} + F_{buoyancy} + F_{DEP} + F_{Coulomb} . \quad (3)$$

Additionally, Brownian motion adds a stochastic component to the dynamics of the wire. We model our nanobelt assembly process using two complementary approaches: analytical expressions and numerical simulations. The analytical expressions are simpler to use than the numerical simulations, but only apply to restricted electrode and particle geometries. When the particles are small relative to the electrode dimensions, the dipole approximation provides a good approximation for the DEP forces. When modeling small particles, the other forces can also be expressed using simple expressions, such as the force on a point charge (Coulomb force), the buoyancy force on a sphere, the drag on a sphere in a low Reynolds number flow (Stokes Law), and the Brownian motion of a sphere in a flow (Stokes-Einstein equation)

$$\begin{aligned} F_{drag} &= 6\pi\eta r u \\ F_{buoyancy} &= (\rho_f - \rho_p)\frac{4}{3}\pi r^3 g \\ F_{Coulomb} &= \frac{q_1 q_2}{d^2} \\ < x^2 >= & \frac{k_b T t}{\pi\eta r} \end{aligned} \quad (4)$$

where η is the fluid viscosity, r is the particle radius, u is the fluid velocity, ρ_f is the fluid density, ρ_p is the particle density, g is gravity, d is the distance between two charges, q_1 and q_2 are point charges on the particle and a second body, and $< x^2 >$ is the expected value of the particle displacement squared. These equations enable a closed form expression for the total force when the velocity field and the electric field are known. Analytical solutions for these fields do exist for some simplified geometries. The flow geometry in a microfluidics device is often a rectangular channel, and in our flow chamber it can be modeled using the parabolic velocity profile of Poiseuille flow

$$u = \frac{\Delta p}{2\eta L}(a^2 - y^2) \quad (5)$$

where Δp is the pressure drop over the channel of length L, y is the vertical position in the channel, and a is the half-height of the channel. A closed form analytical solution for the electric field also exists for a simplified version of the interdigitated array (IDA) electrode often used in DEP. The electric field generated by a periodic array of flat infinitely long electrodes can be expressed using the Schwartz-Christoffel transformation [10].

The analytical modeling of nanowires and nanobelts is more difficult than the modeling of spheres. The force and torque on the wires must be considered simultaneously, the fluid drag and DEP force depend on the orientation of the wire, not only the position. More importantly, the dipole approximation for an ellipsoidal particle [42] is not valid for our geometry, because the wire dimensions are similar to the electrode spacing. This is a requirement in our application since the nanobelts must span across two electrodes to operate as a gas sensor. It may be possible to model the other nanobelt forces and torques using analytical expressions, but no simple expression exists for the DEP force. For this reason, we also perform numerical simulations of the electric field.

The numerical simulations were performed using FEMLAB. FEMLAB is a software package that implements a finite element method to solve partial differential equations. In our computations we use the electrostatics application mode to solve Maxwell's equations for the electric field potential V

$$\nabla^2 V = 0 \quad (6)$$

in two and in three dimensions. Note that the electric field is simply the negative gradient of the electric potential. The boundary conditions on the electrodes are Direchlet boundary conditions for the applied potential; Neumann boundary

(a)

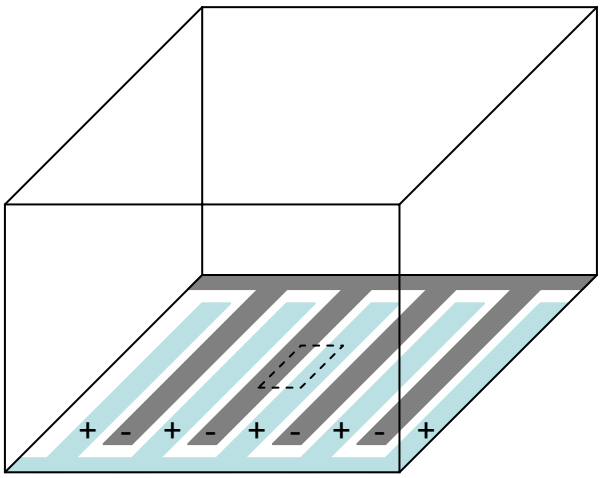

(b)

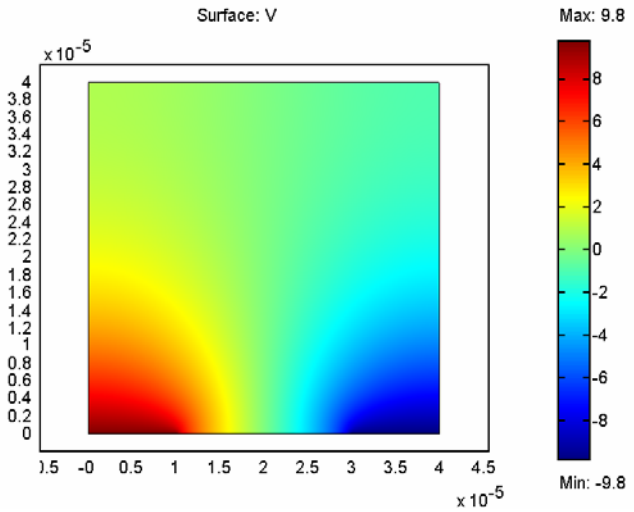

Figure 3. (a) Schematic of the IDA electrode. (b) FEMLAB 2-D simulation for the idealized array. The electric potential *V* is shown, with units in volts. The spatial units are meters.

conditions are used for most other exterior boundaries to model either electrical insulation or symmetry. Interior boundaries were generally modeled with continuity in the electric field displacement, although it is also possible to add a fixed charge to the interior or exterior boundaries. Experimental observations to date do not suggest that charge plays a dominant role relative to the DEP force, but the role of charge and Coulomb forces will be the subject of future work.

Figure 3(a) shows the geometry of the IDA electrode, for which there is an analytical solution [10]. The dashed region of the electrodes is the portion that needs to be modeled in an infinite array of infinitely long electrodes. Figure 3(b) is a FEMLAB simulation of the idealized IDA electrode geometry The interior of the simulation domain represents the fluid, which in our system is ethanol. The simulation represents a two-dimensional slice, in which the rectangular electrodes are infinitely long, infinitesimally thick, and are located along the lower edge of the simulation domain. The positive electrode

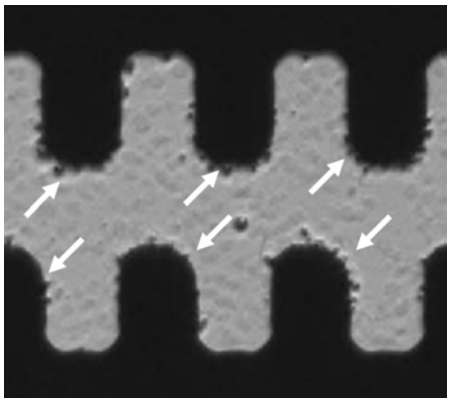

Figure 4. Top-down view of the castellated electrodes. Collection of tin oxide microparticles at a frequency of 1 MHz in ethanol. Arrows indicate concentration of the microparticles.

extends from 0 to 10 μm, the glass substrate is from 10 to 30 μm, and the negative electrode is from 30 to 40 μm. Note that these electrodes have straight edges, as opposed to our castellated electrodes pictured in Figure 4.

The advantage of the numerical simulations is that they can also be used to simulate more complex geometries, such as those presented in Figure 7. The material properties used in the modeling are bulk values from the literature, but their applicability continues to be assessed by comparison between the model and the experiments. For example, the nanobelt dimensions are small relative to the dispersion wavelength of tin oxide [41], so it is possible that the bulk properties of tin oxide will not be accurate.

EXPERIMENTAL OBSERVATIONS

Measurements were made with the electrodes at the bottom and at the top of the measurement cell, so that the gravitational force direction was changed with respect to the electrode array. With the electrodes at the top there was little effect observed for both the nanobelts and microparticles. This is because the gravitational forces dominate over the DEP forces. For the microparticles in ethanol, gravity is greater than DEP force at distances greater than 40 μm from the electrodes (the microchannel height is 80 μm). However with the electrodes at the bottom both microparticles and nanobelts were collected at the electrodes. The SnO_2 microparticles were approximately 1 μm in diameter and were purchased from Alsear Inc. The nanobelts are of interest for our gas sensor arrays, while the microparticle experiments provide a simpler comparison to the modeling, and therefore aid in model development and validation. Note that the masses of the microparticles and nanobelts are similar, although their aspect ratios are very different.

The importance of Brownian motion appears to be small, both for the particles and the nanobelts. This is supported by calculations using equation (4) that show that gravity and buoyancy lead to significantly larger displacements than diffusion. Even though the nanobelts have nanometer scale dimensions, it should be feasible to manipulate them using AC fields. However, we cannot neglect gravity in the assembly

process. It might instead be possible to exploit gravity to aid in the assembly, as in field flow fractionation.

At high frequency (1 MHz) we see lateral attraction of particles to the edges of the castellated electrodes. Without the DEP force the particles were randomly distributed on the glass substrate, however with the DEP forces applied collection was clearly observed, as shown in Figure 4.

The nanobelts are also attracted to the electrodes, but since they span across the electrodes, it is more difficult to visual the spatial force field (which is why we are using particles to assist in building the model). Figure 5 shows effect of high frequency on nanobelts.

At low frequencies (0.1 - 10 Hz) the particles and wires can move substantially during each period, so the fluid drag and DEP forces must be considered together. When the AC voltage is near zero (twice per period), the particles and wires can move due to random disturbances. Images were collected at either 0.25 or 0.5 second intervals. Figure 6 shows the effect of low frequency (1 Hz) excitation with tin oxide microparticles in kerosene. The particles move between the castellated electrodes with low frequency excitation.

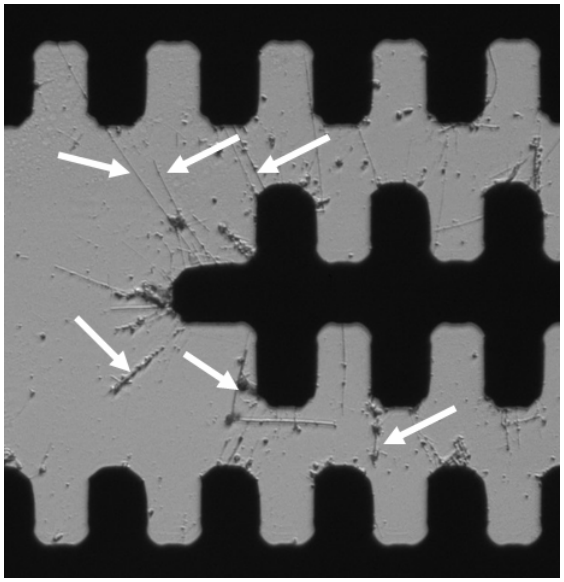

Figure 5: Image of electrode after tin oxide nanobelts are collected at high frequency (1MHz) in kerosene. Similar behavior is observed with nanobelts suspended in ethanol. Arrows indicate the presence of the nanobelts.

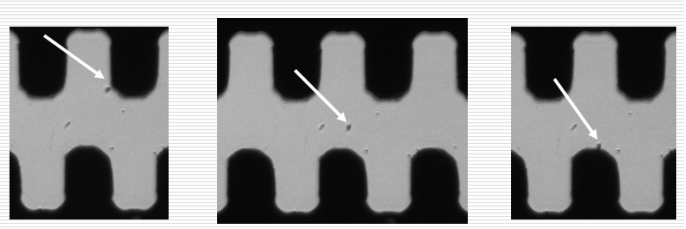

Figure 6: Three frames from the recorded motion of the tin oxide microparticles suspended in kerosene with low frequency (1 Hz) excitation. The arrows indicate the location of the microparticle.

A DC bias of up to 10 V was applied to the electrodes to assess the role of charge and Coulomb forces. The experiment in ethanol was of limited duration (~5 s) due to electrolysis that produced bubbles. Measurements in kerosene where the potential was applied continuously also demonstrated no preferential motion of the microparticles and nanobelts. Because we did not observe attraction to one electrode over the other, which would be expected if the particles or nanobelts were either positively or negatively charged, we can conclude that they are uncharged. If there were some static charge on the wires it would be desirable because it can reduce agglomeration; however the charge did not appear to dominate the DEP forces in our experiments.

SYSTEM DESIGN

The electrode array is used for the nanobelt assembly, but is also an integral part of the final gas sensor. Thus, the assembly process must be designed at the same time as the device. In our study, we begin by fixing the electrode spacing to be approximately the same length as the nanobelts, which is required for gas sensor operation. We then present the results of two other design choices, guided by experiment, modeling, and practical design constraints.

Design of silicon nitride layer

A silicon nitride layer covering the electrodes is desired to prevent electrolysis on the electrodes and to eliminate uncertainty due to oxide formation on the electrodes. The presence of the Si_3N_4 also simplifies the modeling of charge on the assembly surface, since there would only be one fluid-solid interface, instead of two (glass and metal).

However, the film should not significantly reduce the DEP force on the nanobelts. The thickness of the silicon nitride film is one design parameter, as is the permittivity of the fluid. We considered kerosene (relative permittivity of 1.8) and ethanol (25). By comparison the relative permittivity of the silicon nitride is 4. In kerosene, the effect of the film on the electric potential field is negligible for any reasonable film thicknesses, because its permittivity is less than the film, but when using ethanol, the film thickness must be minimized to avoid diminishing the DEP force.

Figure 7 shows two simulations, one with no film, and another with a 1 μm thick film. The effect of the film on the force is quantified by the position of the force contours for a 1 μm diameter particle, using the dipole force formula of equation (1). With no film, the 0.05×10^{11} N contour is at a height of 23 μm above the electrodes. For a 1 μm film, the contour is reduced to 18 μm, a reduction of 22%. For a 500 nm film, the reduction is 11%, and for a 300 nm film the reduction is only 8%. We deposited 300 nm films on our electrode array, which provides only a small reduction of the DEP force and is easily deposited without voids. This electrode array can now be used with either kerosene or ethanol, with little reduction of the DEP force.

Selection of assembly fluid

The previous example showed that the design choices are interrelated, so that the film thickness cannot be selected independently from the assembly fluid. Another consideration in the selection of the assembly fluid is its permittivity and its impact on the DEP force. As given in equations (1) and (2), the DEP force on a spherical particle is proportional to the real part

(a)

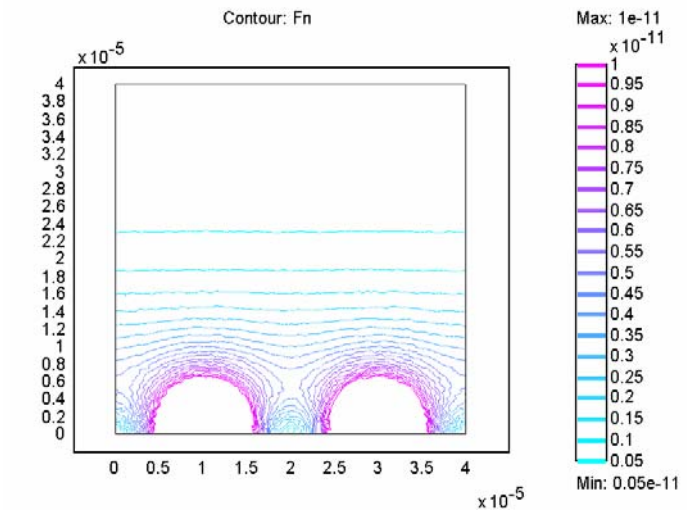

(b)

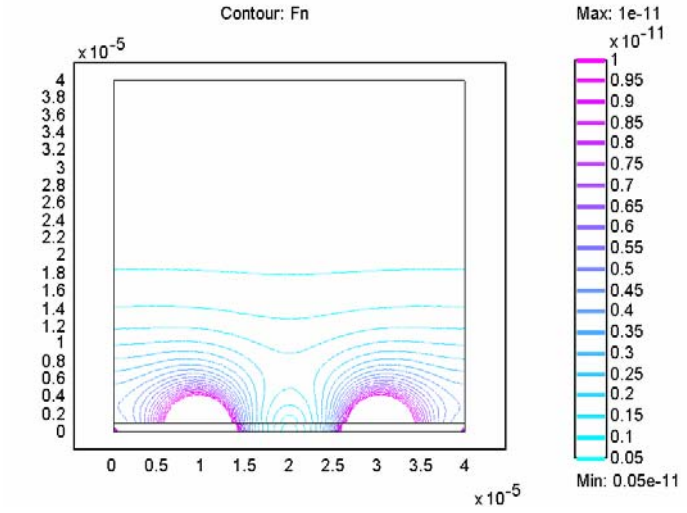

Figure 7. Effect of silicon nitride film thickness on the DEP force. The DEP force (in N) is computed as the absolute value of the dipole force on a 1 μm tin oxide particle in ethanol. (a) No film covering the electrodes. (b) 1 μm thick film of Si_3N_4.

of the fluid permittivity, and is also indirectly affected through the Clausius-Mossotti factor. In our application and for our range of frequencies (0.1 Hz to 1 MHz), the permittivities of the kerosene and ethanol have only real parts. However, the tin oxide is conductive, and we use a reported value of σ=0.1 S/m in our initial modeling. Although the real part of the tin oxide permittivity is 12, the DEP forces are dominated by the imaginary part due to the tin oxide conductivity: $\sigma/(2\pi f \varepsilon_0)$. As a result, over the practical DEP frequency range, the real part of the Clausius-Mossotti factor is 1, and the DEP force in equation (1) is proportional to the fluid permittivity. Thus, we select ethanol over kerosene, yielding forces that are an order of magnitude higher. In the experimental observations, it was suggested that high frequencies will be simpler to analyze and manipulate, due to decoupling from the time-varying fluid forces. At this time, it appears that we can operate with ethanol, a silicon nitride film of 300 nm, and at 1 MHz, with few performance tradeoffs.

CONCLUSIONS AND FUTURE WORK

Strong attraction of tin oxide microparticles and nanobelts has been demonstrated at castellated gold electrodes over a wide frequency range in kerosene and ethanol. There was no significant difference in the general behavior observed indicating that the modeling of the DEP forces are useful and have validity to guide the design of electrode arrays for the assembly of nanobelts. Gravitational forces are significant and play an important role in both kerosene and ethanol. Thus the buoyancy forces are larger than the DEP forces generated over a significant portion of the microchannel volume. The conductivity of the tin oxide particles and nanobelts is such that the frequency dependant DEP force was not detected over the frequency range 0.1- 10 MHz. However, with other materials of lower conductivity, dispersion might well be observed. The effect of a thin dielectric coating of silicon nitride was examined over the electrodes which can reduce electrode fouling. The magnitude of the DEP force was not reduced significantly for a 0.3 μm thick coating and reduced by only 20% for a 1 μm thick layer. These predictive physics based models will provide the tools important for the design of microfluidic systems for the assembly of nanobelts and nanowires. The data produced from targeted experiments provides information for the model building.

The future work will include making quantitative measurements in the experiments by tracking particle velocities as a function of conditions. In addition, a controlled flow orthogonal to the DEP forces to counteract gravity in the experiment will enable observations that quantify collection efficiency as a function of the operating conditions. These microfluidic devices can be then be applied to assembly of tin oxide nanobelts for gas sensors.

ACKNOWLEDGMENTS

We wish to acknowledge the financial support of Nanoscience and Nanotechnology Fellowship Committee of Georgia Institute of Technology for supporting Mr. S. Kumar with a NaST Fellowship, and to the Georgia Tech Nanoscience/Nanoengineering Research Program for additional financial support. The authors would like to thank Swaminathan Rajaraman and the staff of Microelectronics Research Center (MiRC) at Georgia Tech for the clean room facilities used to fabricate electrodes. Special thanks to Dr. Xiangyang Kong for making the nanobelt sample.

[1] Z. L. Wang, Y. Liu, Z. Zhang (eds.), *Handbook of Nanophase and Nanostructured Materials*, Wiley-VCH, New York, 2002.

[2] C. A. Mirkin, R. L. Letsinger, R. C. Mucic, J. J. Storhoff, "A DNA-based method for rationally assembling nanoparticles into macroscopic materials," *Nature,* vol. 382, pp. 607-609, 1996.

[3] C. J. Curtis, D. L. Schulz, A. Miedaner, J. Alleman, T. Rivkin, J. D. Perkins, D. S. Ginley, "Spray and inkjet printing of hybrid nanoparticle-metal-organic inks for Ag and Cu metallizations," *Synthesis, Functional Properties and Applications of Nanostructures Symposium*, MRS Proceedings vol.676, pp. 1-6, 2002.
[4] S. W. Director and W. Maly, *Statistical Approach to VLSI,* North-Holland, Amsterdam, 1994.
[5] B. Ciciani, *Manufacturing Yield Evaluation of VLSI/WSI Systems*, IEEE Computer Society Press, Los Alamitos, California, 1995.
[6] P. J. Burke, "Nanodielectrophoresis: Electronic Nanotweezers," in *Encyclopedia of Nanoscience and Nanotechnology,* Ed: H. S. Nalwa, vol.10, pp. 1-19, American Scientific Publishers, New York, 2003.
[7] R. Pethig, *Dielectric and Electronic Properties of Biological Materials,* Wiley, Great Britain, 1979.
[8] T.B. Jones, *Electromechanics of Particles,* Cambridge University Press, Cambridge UK, 1995.
[9] Y. Huang, K. L. Ewalt, M. Tirado, R. Haigis, A. Forster, D. Ackley, M. J. Heller, J. P. O'Connell, M. Krihak, "Electric manipulation of bioparticles and macromolecules on microfabricated electrodes," *Anal. Chem.,* vol. 73, pp. 1549-1559. 2001.
[10] P. Van Gerwen, W. Laureyn, W. Laureys, G. Huyberechts, M. O. De Beeck, K. Baert, J. Suls, W. Sansen, P. Jacobs, L. Hermans, R. Mertens, "Nanoscaled interdigitated electrode arrays for biochemical sensors," *Sensors and Actuators B,* vol. 49, pp. 73-80, 1998.
[11] W. H. Li, H. Du, D. F. Chen, C. Shu, "Analysis of dielectrophorestic electrode arrays for nanoparticles manipulation," *Computational Materials Science,* vol. 30, pp. 320-325, 2004.
[12] M. R. Diehl, S. N. Yaliraki, R. A. Beckman, M. B. Barahona, J. R. Heath, "Self-assembled, deterministic carbon nanotubes wiring networks," *Angew. Chem. Int. Ed.,* vol. 41, pp. 353-356, 2002.
[13] P. E. Pehrsson, J.W. Baldwin, "Nanotechnology based on diamond and carbon nanotubes," *6th World Multiconference on Systemics, Cybernetics and Informatics. Proceedings, IEEE,* vol.14, pp. 53-58, 2002.
[14] J. Suehiro, G. Zhou, M. Hara, "Fabrication of a carbon nanotubes-based gas sensor using dielectrophoresis and its application for ammonia detection by impedance spectroscopy," *J. Phys. D. Appl. Phys,* vol. 36, pp. L109-L114, 2003.
[15] K. Yamamoto. S. Akita, Y. Nakayama, "Orientation and purification of carbon nanotubes using AC electrophoresis," *J. Phys. D: Appl. Phys.,* vol. 31, pp. L34-L36, 1998.
[16] P. A. Smith, C. D. Nordquist, T. N. Jackson, T. S. Mayer, B. R. Martin, J. Mbindyo, T. E. Mallouk, "Electric-field assisted assembly and alignment of metallic nanowires," *Applied Phys. Lett.* vol. 77, pp. 1399-1401, 2000.
[17] L. A. Nagahara, I. Amlani, J. Lewwnstein, R. K. Tsui, "Directed placement of suspended carbon nanotubes for nanometer-scale assembly," *Appl. Phys. Lett.,* vol. 80, pp. 3826-3828, 2002.
[18] R. Krupke, F. Hennrich, H. B. Beckmann, O. Hampe, S. Makik, M. M. Kappes, H. V. Lohneysen, "Contacting single bundles of carbon nanotubes with alternating electric fields," *Appl. Phys. A,* vol. 76, pp. 397-400, 2003.
[19] M. S. Kumar, S. H. Lee, T. Y. Kim, T. H. Kim, S. M. Song, J. W. Yang, K. S. Naham, E. K. Suh, "DC electric field assisted alignment of carbon nanotubes on metal electrodes," *Solid-State Electronics,* vol. 47, pp. 2075-2080, 2003.
[20] X. Q. Chen, T. Saito, H. Yamada, K. Matsushige "Alligned single-wall carbon nanotubes with an alternating-current electric field," *Appl. Phys. Lett.,* vol. 78, pp. 3714-3716, 2001.
[21] J. Chung, J. Lee, "Nanoscale gap fabrication and integration of carbon nanotubes by micromachining," *Sensors and Actuators A,* vol. 104, pp. 229-235, 2003.
[22] J. Chung. K.-H. Lee, J. Lee, R. S. Ruoff, "Towards large-scale integration of carbon nanotubes," *Langmuir,* vol. 20, pp. 3011-3017, 2004.
[23] Z. Chen, Z. Du, M.-H. Du, C. D. Rancken, H.-P. Cheng A. G. Rinzler, "Bulk separative enrichment in metallic or semiconducting single-walled carbon nanotubes," *Nanoletters,* vol. 3, pp. 1245-1249, 2003.
[24] D. S. Lee, D. W. Kim, H. S. Kim, S. W. Lee, S. H. Jhang, Y. W. Park, E. E. B. Campbell, "Extraction of semiconducting CNTs by repeated dielectrophoretic filtering," *Appl. Phys. A.,* vol. 80, pp. 5-8, 2005.
[25] S.Jin, D. Whang, M. C. McAlpine, R. S Freidman, Y. Wu, C. M. Lieber, "Scalable interconnection and integration of nanowire devices without registration," *Nanoletters,* vol. 4, pp. 915-919, 2004.
[26] T.C. Pearce, S. S. Schiffman, H. T. Nagle, J. W. Gardner, *Handbook of Machine Olfaction – Electronic Nose Technology,* Wiley-VCH, Weinheim, Germany, 2003.
[27] J. W. Gardner, V. K. Varadan, O. O. Awadelkarim, *Microsensors, MEMS and Smart Devices*, John Wiley & Sons, New York, 2001.
[28] S. R. Morrison, S. R. *The Chemical Physics of Surfaces,* Plenum Press, New York, 1978.
[29] S.-C. Chang, S.-C, and Hicks, D. B., "Tin Oxide Microsensors on Thin Silicon Membranes," in *Digest of Technical Papers, IEEE Solid-State Sensors Workshop*, Hilton Head, SC, IEEE, New Jersey, 1986.
[30] Y. Cui, Q. Q. Wei, H. Park, C. M. Lieber, "Nanowire nanosensors for highly sensitive and selective detection of biological and chemical species," *Science,* vol. 293, pp. 1289-1292, 2001.
[31] E. Comini, G. Faglia, and G. Sberveglieri, Z. Pan and Z. L. Wang, "Stable and highly sensitive gas sensors based on semiconducting oxide nanobelts" *Applied Physics Letters*, vol. 81, pp. 1869-1872, 2002.
[32] Y. M. Wong, W. P. Kang, J. L. Davidson, A. Wisitsora-at, K. L. Soh, "A novel microelectronic gas sensor utilizing carbon nanotubes for hydrogen gas detection," *Sensors and Actuators B,* vol. 93, pp. 327-332, 2003.
[33] D. Zhang, Z. Liu, C. Li, T. Tang, X. Liu, S. Han, B. Lei, C. Zhou, "Detection of NO_2 down to ppb levels using

individual and multiple In_2O_3 nanowire devices," *Nano Letters,* vol. 4, pp. 1919-1924, 2004.
[34] C. Li, B. Lei, D. Zhang, X. Liu, S. Han, T. Tang, M. Rouhanizadeh, T. Hsiai, C. Zhou, "Chemical gating of In_2O_3 nanowires by organic and biomolecules," *Appl. Phys. Lett.,* vol. 83, pp. 4014-4016, 2003.
[35] F. Patolsky, G. Zheng, O. Hayden, M. Lakadamyali, X. Zhuang, C. M. Lieber, "Electrical detection of single viruses," *PNAS,* vol. 101, pp. 14017-14022, 2004.
[36] L. Zheng, S. Li, P. J. Burke, "Self-assembled gold nanowires from nanoparticles: an electronic route towards DNA nanosensors," *Proceedings of the SPIE* vol. 6, pp. 5515-5519, 2004.
[37] Shi, L. , Q. Hao, C. Yu, N. Mingo, X. Kong, Z. L. Wang, "Thermal conductivities of individual tin dioxide nanobelts," *Appl. Phys. Lett.* vol. 84, pp. 2638-2640, 2004.
[38] Z. W. Pan, Z. R. Dai, Z.L. Wang, "Nanobelts of semiconducting oxides," *Science,* vol. 291, pp. 1947-1949, 2001.
[39] Z. R. Dai, Z. W. Pan, Z. L. Wang, "Novel Nanostructures of Functional Oxides Synthesized by Thermal Evaporation," *Adv. Funct. Mater.,* vol. 13, pp. 9-24 , 2003.
[40] Z.L. Wang, "Nanobelts, Nanowires and Nanodiskettes of Semiconducting Oxides – from materials to nanodevices," *Adv. Mater.,* vol. 15, pp. 432-436, 2003.
[41] S. Rajaraman, H.-S. Noh, P. J. Hesketh, D. S. Gottfried "Rapid, low cost microfabrication technologies toward realization of devices for dielectrophoretic manipulation of particles and nanowires," in press, *Sensors and Actuators,* 2005.
[42] M. Dimaki, P. Boggild, "Dielectrophoresis of carbon nanotubes using microelectrodes: a numerical study," *Nanotechnology,* vol. 15, pp. 1095-1102, 2004.
[41] A. E. Rakhshani, Y. Makdisi, and H. A. Ramazaniyan, "Electronic and optical properties of fluorine-doped tin oxide films," *J. Appl. Phys.,* vol. 83, pp. 1049-1057, 1998.